

GA-A27321

**FAST PEDESTAL, SOL, AND DIVERTOR
MEASUREMENTS FROM DIII-D TO VALIDATE
BOUT++ NONLINEAR ELM SIMULATIONS**

by

**M.E. FENSTERMACHER, X.Q. XU, I. JOSEPH, M.J. LANCTOT, C.J. LASNIER,
W.H. MEYER, B.J. TOBIAS, L. ZENG, A.W. LEONARD, and T.H. OSBORNE**

MAY 2012



DISCLAIMER

This report was prepared as an account of work sponsored by an agency of the United States Government. Neither the United States Government nor any agency thereof, nor any of their employees, makes any warranty, express or implied, or assumes any legal liability or responsibility for the accuracy, completeness, or usefulness of any information, apparatus, product, or process disclosed, or represents that its use would not infringe privately owned rights. Reference herein to any specific commercial product, process, or service by trade name, trademark, manufacturer, or otherwise, does not necessarily constitute or imply its endorsement, recommendation, or favoring by the United States Government or any agency thereof. The views and opinions of authors expressed herein do not necessarily state or reflect those of the United States Government or any agency thereof.

GA-A27321

FAST PEDESTAL, SOL, AND DIVERTOR MEASUREMENTS FROM DIII-D TO VALIDATE BOUT++ NONLINEAR ELM SIMULATIONS

by

M.E. FENSTERMACHER,* X.Q. XU,* I. JOSEPH,* M.J. LANCTOT,* C.J. LASNIER,*
W.H. MEYER,* B.J. TOBIAS,[†] L. ZENG,[‡] A.W. LEONARD, and T.H. OSBORNE

This is a preprint of a paper to be presented at the Twentieth International Conference on Plasma-Surface Interactions in Controlled Fusion Devices, May 21–25, 2012 in Aachen, Germany and to be published in the *J. Nucl. Mater.*

*Lawrence Livermore National Laboratory, Livermore, California, USA.

[†]Princeton Plasma Physics Laboratory, Princeton, New Jersey, USA.

[‡]University of California Los Angeles, Los Angeles, California, USA.

Work supported by
the U.S. Department of Energy under
DE-AC52-07NA28344, DE-AC02-09CH11466,
DE-FG02-08ER54984, and DE-FC02-04ER54698

GENERAL ATOMICS PROJECT 30200
MAY 2012



Paper P1-009

Fast Pedestal, SOL and Divertor Measurements from DIII-D to Validate BOUT++ Nonlinear ELM Simulations

M.E. Fenstermacher^{a*}, X.Q. Xu^a, I. Joseph^a, M.J. Lanctot^a, C.J. Lasnier^a, W.H. Meyer^a,
B. Tobias^b, L. Zeng^c, A.W. Leonard^d and T.H. Osborne^d

^a*Lawrence Livermore National Laboratory, Livermore, California 94550, USA*

^b*Princeton Plasma Physics Laboratory, Princeton, New Jersey 08543, USA*

^c*University of California-Los Angeles, Los Angeles, California 90095-7099, USA*

^d*General Atomics, San Diego, California 92186-5608 USA*

Abstract. This paper documents first work toward validation of BOUT++ nonlinear edge localized mode (ELM) simulations in X-point geometry, at experimental pedestal collisionality, against multiple diagnostic measurements of a well-characterized ELM event in DIII-D. The key to the BOUT++ simulations is the use of a hyper-resistivity model that effectively spreads the very thin current sheets that form in low collisionality nonlinear simulations, and allows for ELM driven magnetic reconnection at finite current density. Experimental ELM characterization includes multiple 1-D fast diagnostic measurements revealing in-out divertor asymmetric response to ELMs, 2D IRTV at the divertor targets, 3D visible emission in the divertor volume to test the extension of BOUT++ to X-point geometry, and forward modeling of new 2D electron cyclotron emission imaging to test predictions of ELM filaments in the edge pedestal. Initial comparisons show qualitative agreement between BOUT++ results and several measurements.

PACS: 52.55.Fa, 52.55.Rk, 52.70.Kz, 52.65.Kj

1. INTRODUCTION

The impulsive heat and particle losses due to unmitigated Type-I edge localized modes (ELMs) [1] are predicted to cause excessive erosion and damage to plasma facing components (PFCs) in future high power tokamak devices [2, and references therein]. Full nonlinear predictive capability for ELM energy loss, target heat flux deposition etc. would be very valuable to predict PFC requirements for future reactor designs, and requirements for candidate ELM control techniques. Previously ELM simulations were limited to artificially high collisionality regimes due to numerical problems associated with very thin current sheets that form in low collisionality nonlinear simulations. A new hyper-resistivity model in the BOUT++ fluid MHD code [3] allows full nonlinear simulations at experimental collisionality, and therefore permits direct comparison of code predictions with multiple experimental measurements. The purpose of this paper is to document initial progress toward validation of this BOUT++ model, extended to X-point geometry, with fast ELM measurements on DIII-D.

The paper is organized as follows. The experimental characterization of ELM events in the DIII-D tokamak is given in Sec. 2. The results of linear and nonlinear BOUT++ simulations of this ELM are described in Sec. 3. A comparison of the initial simulation results with some of the experimental measurements is discussed in Sec. 4 leading to preliminary conclusions and plans for future validation work.

2. EXPERIMENTAL ELM CHARACTERIZATION

The Type-I ELM characterized in this paper occurred in the standard ELMing H-mode phase of a discharge. Later in the discharge the plasma was subjected to significant $n = 2$ resonant magnetic perturbations (RMPs) that completely suppressed the Type-I ELMs [4]. The work reported here is the beginning of a continuing project to validate nonlinear BOUT++ simulations of both standard Type-I ELMs dynamics and the effects of RMPs to achieve ELM suppression. The lower single-null (LSN) equilibrium plasma shape and evolution of basic plasma parameters for the DIII-D discharge are shown in Fig. 1. Steady-state conditions during the ELMing H-mode phase without the RMP were $I_p = 1.5$ MA, $B_T = 1.95$ T, average $P_{NBI} = 5.6$ MW, $R = 1.75$ m, $a = 0.6$ m, $\kappa = 1.82$, $\delta = 0.65$, $q_{95} = 3.64$, and $\beta_N = 2.0$. Regular T-I ELMs at 40 Hz occurred from 2.0–2.4 s.

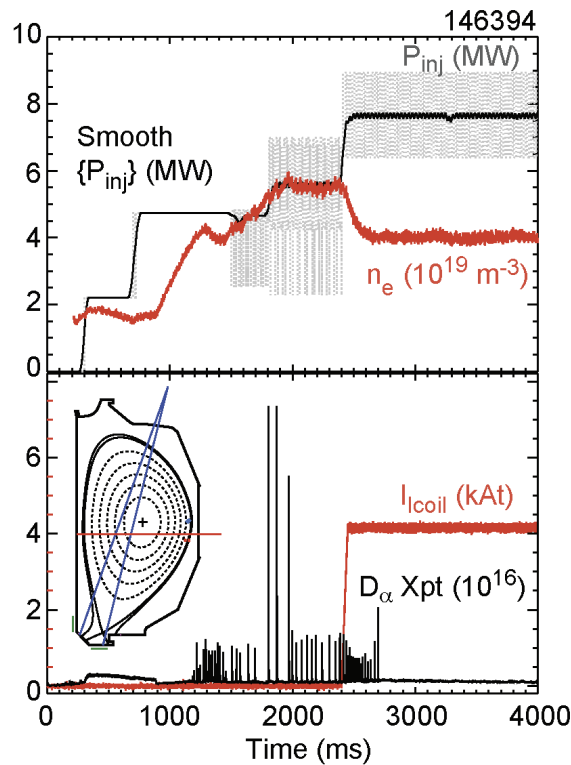


Fig. 1. Evolution of key parameters for DIII-D discharge 146394 from which the ELM at 2241 ms was simulated with BOUT++, including (a) neutral beam power (MW) and line averaged density (10^{19} m $^{-3}$), and (b) I-coil current (kAt) and outer divertor D_α emission (au). Insert shows equilibrium shape and diagnostic locations for signals in Fig. 2.

The crash and recovery of the ELM at 2241 ms (Fig. 2) were detected with multiple fast acquisition data chords in the pedestal, scrape-off layer (SOL) and divertor; this provides a significant database for validation of a BOUT++ nonlinear simulation of this instability event. Figure 2(a) shows that this ELM produced a drop in the plasma stored energy of 6.5% (72 kJ from a 1.1 MJ plasma) and a reduction of the line integrated density of 5%. Fast transients were seen on an electron cyclotron emission (ECE) channel at the top of the pedestal, and on the outer midplane tangential D_α channels [Fig. 2(b)], which showed a larger transient in the SOL than at the pedestal top. Transients seen in the divertor included an immediate spike in the D_α chord viewing the low field side (LFS) X-point region, and a delayed, smaller response from the chord viewing the inner divertor leg [Fig. 2(c)], perhaps indicating burn-through of the detached inner leg during ELMs. The response of CIII (465 nm) emission [Fig. 2(d)] was larger from the inner divertor chord than from the outer X-point measurement, as was the response of j_{sat} from a target mounted probe near the inner strike point (ISP) vs the outer strike point

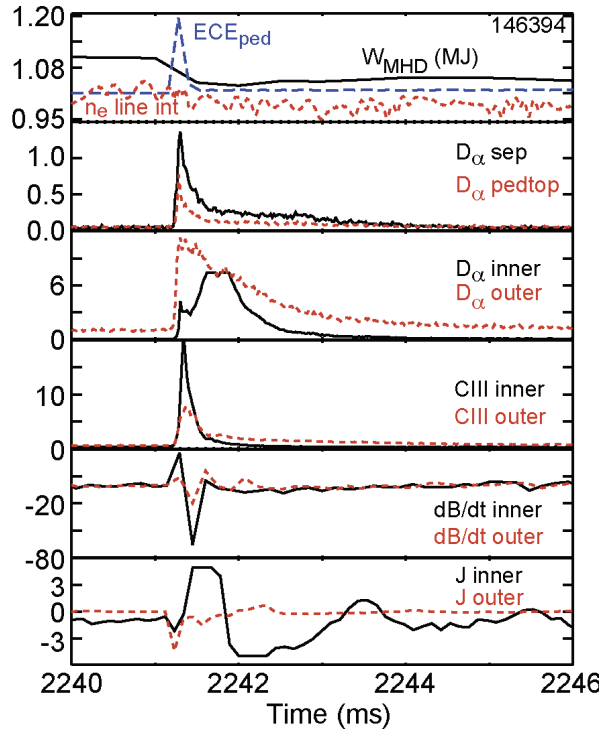


Fig. 2. Evolution of multiple local measurements during the Type-I ELM at 2241.15 ms including (a) total stored energy (MJ), line-integrated density along a horizontal midplane chord (10^{19} m^{-2}) and ECE emission near the top of the pedestal, (b) D_α emission from the top of the pedestal and near the separatrix at the LFS midplane, (c) D_α and (d) CIII (465 nm) emission from the ISP and LFS X-point, (e) dB/dt (T/s), and (f) ion saturation current (j_{sat}) from the ISP and OSP.

(OSP) strike-point [Fig. 2(f)]. However the response on a magnetic probe below the floor near the OSP was larger than the corresponding response of a magnetic probe near the ISP [Fig. 2(e)]. Finally, fast reflectometry profile measurements Fig. 3 showed the initial drop of pedestal density and broadening into the SOL, followed by rapid recovery of the SOL and gradual pedestal build-up. These measurements provide data to test multiple aspects of the ELM dynamics in the BOUT++ physics model.

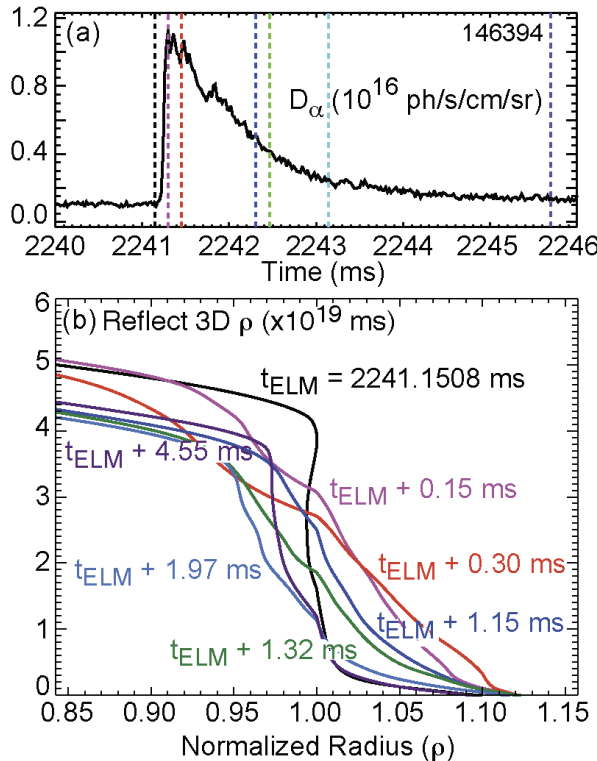


Fig. 3. Evolution of edge electron density profiles during the ELM with (a) temporal evolution from D_α emission in the outer divertor leg, and (b) multiple n_e profiles at times during the ELM evolution marked by vertical dashed lines in (a).

The effect of the ELM crash was also observed on several 2D and 3D diagnostics, including divertor IR emission showing broadening of heat deposition with multiple helical structures, and tangentially viewing visible emission showing broadening of the carbon emission in the divertor. In Fig. 4(a) the data from the infrared television (IRTV) show that the ELM event causes a substantial increase of the target temperature far into both the inner and the outer SOL regions, including multiple helical striations of the temperature as seen in other devices [5]. In Fig. 4(b,c) CIII emission (465 nm) data show that the ELM broadens the visible emission profile substantially into the SOL at both the ISP and OSP.

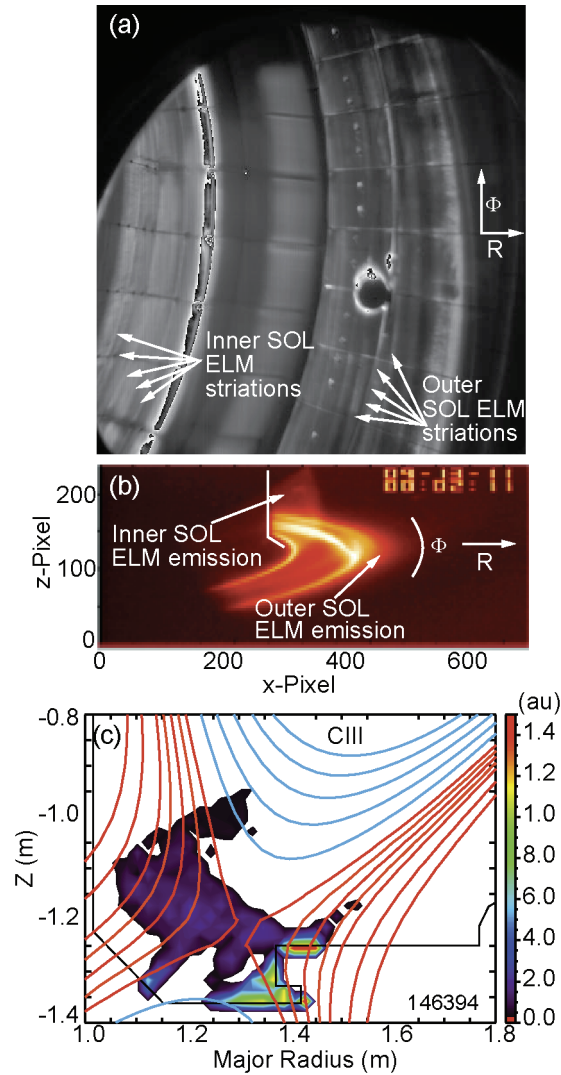


Fig. 4. ELM signatures on 2D diagnostics with (a) temperature change on the divertor target from IRTV data, (b) 3D CIII (465 nm) emission and (c) 2D reconstructions of the CIII profile during the ELM from tangentially viewing camera data.

3. BOUT++ LINEAR AND NONLINEAR ELM SIMULATIONS

The ELM simulations in this paper were done with a three-perturbation-field (magnetic flux \tilde{A}_{\parallel} , electric potential $\tilde{\Phi}$, and pressure \tilde{p}) model [3] extracted from the complete BOUT++ two fluid MHD equations. Non-ideal effects (finite resistivity- $\nabla_{\perp}^2 A_{\parallel}$, diamagnetic drift, $E \times B$ drift, anomalous perpendicular viscosity and parallel viscosity and thermal diffusivity) are retained and a hyper-resistivity or electron viscosity term ($\nabla_{\perp}^4 A_{\parallel}$) is added to facilitate ELM magnetic reconnection with finite current sheets at the low resistivity in experiments. The magnitude of the hyper-resistivity term is set by the assumption that the anomalous electron viscosity is comparable to the anomalous electron perpendicular thermal diffusivity (Prandtl number close to unity). The three-field equations are solved using a field-aligned (flux) coordinate system with shifted radial derivatives [6] on a periodic domain in the parallel coordinate (with a twist-shift BC) and in toroidal angle.

The BOUT++ ELM simulations, for comparison with the measured ELM effects above, were run with as many of the input parameters as possible taken from experimental measurements. The kinetic plasma profiles needed for the calculation were obtained by averaging data from the last 70% of the ELM cycle for the ELM at 2241 ms. Figure 5(a-d) show the fitted profiles of n_e , T_e , p_e from Thomson scattering measurements, T_i , toroidal rotation, poloidal rotation and radial electric field (E_r) from charge exchange recombination (CER) data, and the edge current profile including the bootstrap contribution calculated from the data fits using the Sauter formula [7]. These profiles, plus core current profile data from motional Stark effect (MSE) measurements, were used to generate the kinetic EFIT equilibrium that provided the flux surface geometry for the simulations.

BOUT++ linear simulations indicated that the plasma in the last 20% of the ELM cycle before the ELM crash was unstable to peeling-balloon modes, in agreement with independent linear stability calculations from the ELITE code [8]. The BOUT++ linear simulation show $n = 25$ that the growth rate peaks for toroidal modes between $n = 15$ and $n = 20$, with a radial mode structure that displays both a broad ballooning feature for $0.9 < \Psi_N < 0.97$, and a narrow peeling feature at the edge for $\Psi_N > 0.97$ [Fig. 6(a)]. A parallel viscosity in the range $3.3-6.7 \times 10^7$ m²/s was necessary to obtain convergence of the peeling mode structure near the X-point.

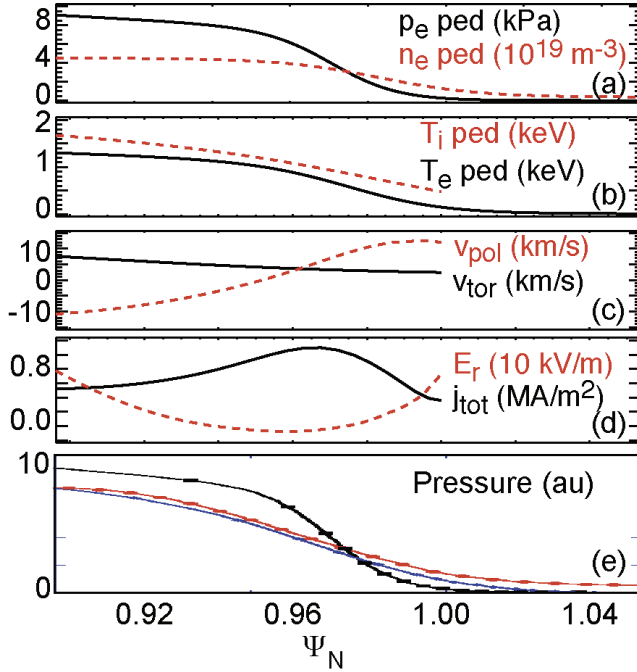


Fig. 5. Curve fits to pre-ELM radial profiles of plasma parameters in the pedestal from Thomson scattering and CER data including (a) electron pressure (kPa) and density (10^{19} m^{-3}), (b) electron and C^{+6+} ion temperatures (keV), (c) toroidal and poloidal rotation (km/s) and (d) radial electric field ($E_r - \text{kV/m}$) and edge current density including the bootstrap contribution (MA/m^2). In (e) a comparison of profiles of measured pre-ELM (black) and pos-ELM (blue) electron pressure, vs the BOUT++ simulated post-ELM pressure (red) normalized to the post-ELM data at $\Psi_N = 0.9$.

The initial BOUT++ nonlinear simulations show rapid saturation of the ELM pressure perturbation and propagation of the ELM structure into the SOL near the outer midplane. The ELM crash time is about 20 Alfvén times, or about $3 \mu\text{s}$, and multiple filaments are observed especially near the X-point [Fig. 6(b)]. The radial profile of the simulated pressure perturbation at the outer midplane is very similar to the coherent average of the profile data from the first 10% of the ELM cycle [Fig. 5(e)].

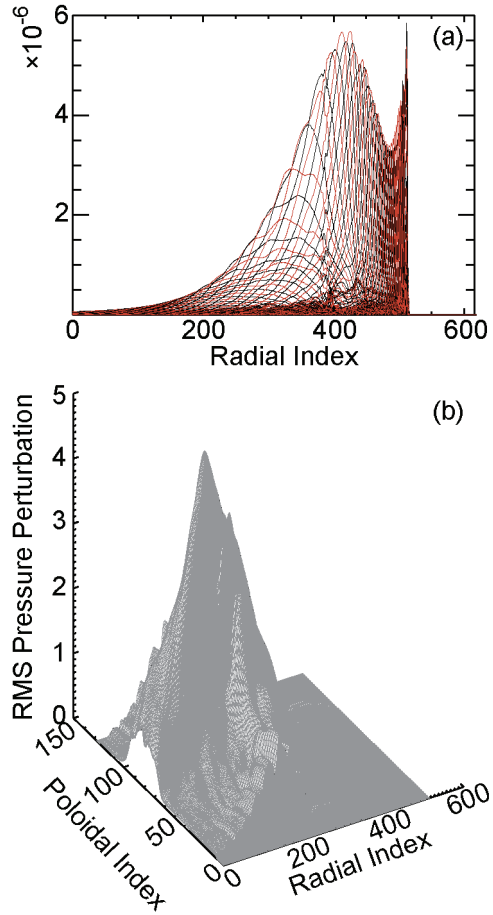


Fig. 6. BOUT++ results including (a) radial structure of poloidal harmonics for $n = 25$ dominant linear instability mode, and (b) 2D structure at an initial nonlinear ELM crash.

4. DISCUSSION AND OUTLOOK

The DIII-D fast diagnostic set provides multiple measurements of the evolution of the pedestal, SOL and divertor plasmas during an ELM cycle for validation of BOUT++ linear and nonlinear ELM simulations. Recent data includes inner vs outer 1D fast chordal data, plus fast 2D and 3D images; additional ELM measurements can be obtained by optimizing future experiments. Substantial synthetic diagnostic development work is underway to allow BOUT++ solutions to be directly compared with many of these measurements. This includes a parallel heat flux model needed to compare with IR data, carbon radiation models to compare with the filtered TV data, and models of the magnetic probe response to the BOUT++ ELM induced profile evolution.

Future work to validate BOUT++ ELM simulations will also include comparison of predicted ELM emission structure with data from ECEI in the pedestal and images (both IR and line filtered visible emission from a new tangentially viewing periscope installed on DIII-D. Figure 7(a) shows the predicted ECEI profile by forward modeling the $n = 25$ linear mode from BOUT++. ECEI was cutoff for the ELMing period analyzed here, but ECEI profiles very similar to this modeling were seen in similarly prepared plasmas at slightly lower density below cutoff [9]. Figure 7(b) shows a 3D rendering of the same BOUT++ linear mode as it will be viewed with the visible/IR periscope in future experiments. Past experiments in DIII-D with a limited poloidal view of the edge [10] have shown that ELM CIII emission from the SOL can compare well with calculated linear ELM structure from ELITE. The wide-angle poloidal view of CIII emission from the new periscope will provide another strong test of BOUT++ linear and nonlinear predictions of the 3D ELM structure.

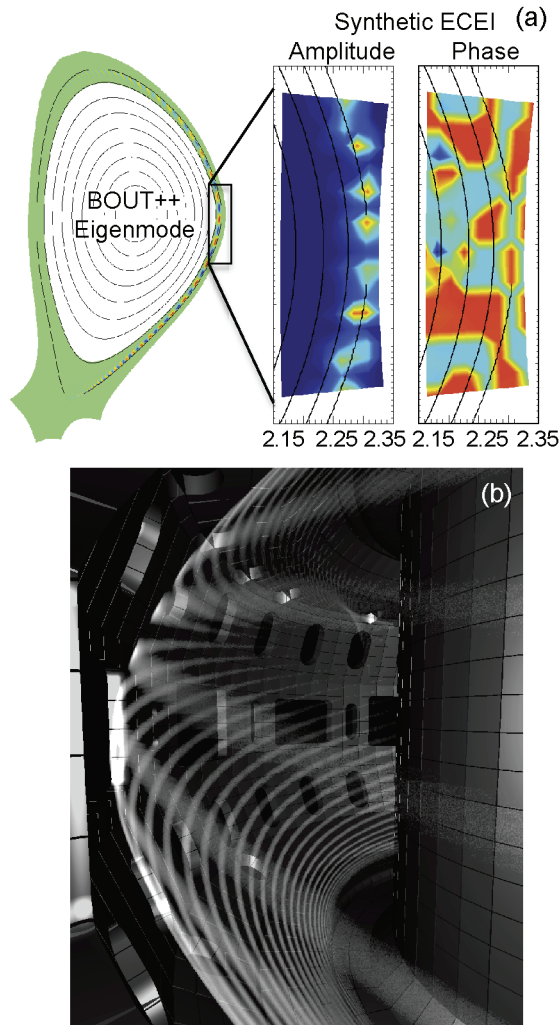


Fig. 7. 3D projections of an $n = 25$ linear mode from BOUT++ including (a) predicted ECEI emission profile with features near the separatrix anti-correlated to the perturbation and (b) expected CIII emission structure in the midplane tangential view of the new IR/Visible periscope.

REFERENCES

- [1] H. Zohm, Plasma Phys. Control. Fusion **38**, 105 (1996).
- [2] A. Loarte *et al.*, Proc. 23rd IAEA Fusion Energy Conference, Daejeon, Korea (2010).
- [3] X.Q. Xu *et al.*, Nucl. Fusion **51**, 103040 (2011).
- [4] M.J. Lanctot *et al.*, “Complete Suppression of Large Type-I Edge Localized Modes Using Multi-harmonic Magnetic Perturbations in DIII-D,” submitted for publication in Nucl. Fusion (2012).
- [5] T. Eich *et al.*, J. Nucl. Mater. **337**, 669 (2005).
- [6] B. Dudson, Comput Phys Commun, **180**, 1467 (2009).
- [7] O. Sauter, C. Angioni, and Y.R. Lin-Liu, Phys. Plasmas **6**, 2834 (1999).
- [8] P.B. Snyder, H.R. Wilson, and X.Q. Xu, Phys. Plasmas **12**, 056115 (2005).
- [9] B. Tobias *et al.*, “ECE-Imaging of the H-mode Pedestal” submitted to Rev. Sci Instrum (2012).
- [10] M.E. Fenstermacher *et al.*, Nucl. Fusion **45**, 1493 (2005).

ACKNOWLEDGMENT

This work was supported in part by the US Department of Energy under DE-AC52-07NA27344, DE-AC02-09CH11466, DE-FG02-08ER54984, and DE-FC02-04ER54698.